Inelastic deuteron scattering in the Coulomb nuclear interference region: Procedures for estimating the precision of the extracted $B(E2)$ and $B(IS2)$ values

J. L. M. Duarte, G. M. Ukita, T. Borello-Lewin, L. B. Horodynski-Matsushigue, and L. C. Gomes
Instituto de Física, Universidade de São Paulo, Caixa Postal 66318, 05389-970, São Paulo, SP, Brazil
(Received 3 September 1996; revised manuscript received 28 February 1997)

Taking ^{94}Mo$(d,d')^{94}$Mo(2_1^+) at 13.2 MeV incident energy as an example, a discussion is made about the influence of known experimental uncertainties in the primary data on the precision of the $B(E2)$ and $B(IS2)$ values, extracted in Coulomb-nuclear interference (CNI) measurements in a correlated way. The reflexes of judicious variations of three optical model parameters (around the global prescription) on the extracted values are also examined. The good quality of the data obtained with the S. Paulo Pelletron-Enge-Spectrograph facility is shown to allow for a 2–3 % statistical uncertainty level for these quantities, within a distorted-wave Born approximation-deformed optical model approach. The accuracy of relative values of the ratio $B(E2)/B(IS2)$, which may be linked to the ratio of proton to neutron quadrupole moments, is argued to be of similar order. [S0556-2813(97)04810-3]

PACS number(s): 21.10.Re, 24.10.Ht, 25.45.De, 27.60.+j

I. INTRODUCTION

The literature shows scarce information on isoscalar reduced transition probabilities $B(ISL)$, in contrast to the corresponding quantities $B(EL)$ associated to the charge. Differences, in particular for 2_1^+ states of even nuclei, between $B(E2)$ and the $B(IS2)$ values would reflect unhomogeneous contributions of protons and neutrons to these excitations, which have been extensively used as indicators of nuclei structure properties [1]. Although experimental and theoretical studies [2,3] point to a dominance of simple homogeneous collective effects on most of these quadrupolar excitations, resulting in relative contributions of protons and neutrons of about Z/N, it is clear that a better pinning down of the uncertainties associated, both to the experimental information and to the method of analysis, can reveal explicit differences, of theoretical interest. In particular, it is expected that near single closed shells, protons and neutrons should contribute differently to the 2_1^+ excitation, in spite of core polarization effects [3].

Coulomb-nuclear interference (CNI) in inelastic scattering, with projectiles of isoscalar character, has long been known as an excellent instrument for the simultaneous measurement of $B(EL)$ and $B(ISL)$, since a relative normalization of the results is intrinsically given. Medium energy deuterons are convenient projectiles for the investigation of the 2_1^+ states through CNI studies. In fact, global optical potentials, important ingredients for the macroscopic analysis of inelastic scattering, besides well tested on elastic scattering, were, for deuterons, also extensively applied to several kinds of distorted-wave Born approximation (DWBA) analyses, thereby allowing regions of validity to be established, thus reducing the number of free parameters. In general, the intense collective first quadrupolar excitations are well described by the simple deformed optical model (DOMP) interpretation [4]. This method, if applied in the CNI region, allows the simultaneous extraction of the potential deformation length $\delta^{\rm pot}$, and the charge deformation length δ^C. As usual in DOMP analyses, $\delta^{\rm pot}$ is assumed equal to the nuclear or mass deformation length, which, in turn, specializing for quadrupolar excitations, with isoscalarly interacting projectiles is related to the isoscalar reduced transition probability $B(IS2)$ by

$$B(IS2)=(\delta^{IS})^2\left[\frac{3ZR_m}{4\pi}\right]^2,$$

with $\delta^{IS}\equiv\delta^{\rm pot}$, as supposed.

An analogous relation [5] transforms δ^C:

$$B(E2)\uparrow=(\delta^C)^2\left[\frac{3ZeR_c}{4\pi}\right]^2,$$

where $R_m=r_mA^{1/3}$ and $R_c=r_cA^{1/3}$ are, respectively, the characteristic radii of the mass and the charge distributions of the nucleus. Taking into account this direct quadratic relationship between the reduced transition probabilities and the deformation lengths, which are extracted in the DOMP analyses, the latter ones may be used equivalently in the physical discussion, as will be done in the present paper.

Our group which investigates nuclear structure properties with light ions at the University of São Paulo Pelletron Laboratory was, to our knowledge, the first to use CNI measurements with deuterons. The mass region between $A=90$ and $A=104$ has received our particular attention and disclosed interesting effects [6–8]. In general, differences between mass and charge deformations amount to about 10 to 20%, indicating the necessity of a rather detailed knowledge of the uncertainties which affect these physical informations. There are at least two sources of uncertainties in the extraction of the deformation lengths, if the macroscopic DWBA analysis is taken as sufficiently well founded. One is directly associated to the experimental errors, characteristic of the data taking procedure. The other reflects the uncertainties in the several parameters needed for the theoretical description of the process. Detailed data of the ^{94}Mo$(d,d')^{94}$Mo(2_1^+) reaction

recently obtained [8] at 13.2 MeV incident energy are here taken as example in discussing the methods applied in the effort of obtaining reliable uncertainties for the deformation lengths. On this issue, the present work focuses attention on the reflexes of the experimental statistical errors on the δ^{IS} and δ^{C} values, which are extracted in the CNI studies in a correlated way. These are investigated comparing the outcome of a Monte Carlo simulation around the data points of the experimental angular distribution, in accordance with their standard deviations, with the application of statistical recipes [9], up to now not in common use in nuclear physics analyses. It is to be stressed that in the effort of quantifying uncertainties for the results of experimental nuclear structure studies, it is mandatory, in first place, to be able to represent correctly the influence of the inherent statistical uncertainties, which are always present in the data, since these are, in principle, unambiguously attributed (obtaining thus uncertainties of type A). The recipes should be applicable also to other experimental situations in nuclear physics where two or more correlated parameters are of importance.

A second step towards a complete quantifications of the uncertainties of the $B(E2)$ and $B(IS2)$ would be to obtain trustworthy values for the uncertainties of type B, in particular for the several systematic errors due to the incomplete description of the intervening reaction mechanism. This is outside the scope of the present work. Only the effects of small variations of three optical model parameters, taken as the most relevant for the analysis of medium energy deuteron inelastic scattering, on the DWBA-DOMP outcomes were also taken under consideration. The objective is, up to now, to inspect especially chains of isotopes and isotones near closed shells and in known transitional regions of nuclear structure in a comparative way. In particular, ^{94}Mo is to be compared to ^{98}Mo and both to ^{92}Zr and ^{96}Zr, respectively, in a research program which is still in progress.

II. EXPERIMENTAL PROCEDURE

The experimental setup and precautions in the data-taking process will be presented here in some detail for the example chosen, ^{94}Mo$(d,d')^{94}$Mo(2_1^+), since they are typical for the procedures developed for the CNI studies with deuterons.

The deuteron beam of the São Paulo Pelletron accelerator, with an incident energy of 13.2 MeV, was focused on a ^{94}Mo enriched target, after passing defining slits of 1.0 $\times 2.0$ mm^2, which guarantee an adequate object for the Enge split-pole spectrograph. Through patient focusing, ratios between current on the object defining slits and beam on target of about 1:30 could be achieved and maintained. On a circular slit of ~ 6 mm diameter, situated about half a meter before the defining slits, a ratio of about 1:100 with respect to the beam was pursued, in further guarantee of an adequate profile of the beam. The very uniform target, enriched to $(93.9 \pm 0.1)\%$ and with a thickness of 32 μg/cm^2, was prepared [10] by electron bombardment evaporation of Mo metal, in powder form, on ~ 10 μg/cm^2 carbon backings.

The ejectiles of the reaction were momentum analyzed by the spectrograph and detected at the focal plane in nuclear emulsion (Ilford G.5, 50 μm thick). The use of nuclear emulsion reduces dramatically the background associated with deuteron beams, since these detectors do not respond to the abundant γ and x rays provenient mostly from (n,γ) reactions in the spectrograph iron core, after deuteron breakup. The emulsion plates were scanned, after processing, in strips of 200 μm across the plates.

Figure 1 displays the relevant portion of three spectra ($\theta_{\rm lab} = 14°$, 18°, and 58°), showing the peak associated with the 2_1^+ excitation of ^{94}Mo, at 871.1 keV [11]. Two of the spectra are typical for data taken at forward scattering angles, the good energy resolution of ~ 8 keV full width at half maximum (FWHM), being essential for evidencing the peak with respect to the background, which is due basically to the elastic tail. This background drops rapidly with increasing angle and, at $\theta_{\rm lab} = 58°$, the small peak associated to the ^{95}Mo$(d,d')^{95}$Mo$(\frac{9}{2}^+)$ excitation is clearly observed at the correct energy [12], in the proportion expected from the presence of ^{95}Mo in the target material. The horizontal opening angle of the spectrograph was maintained fixed, corresponding to $\Delta\theta_{\rm lab} = \pm 1.9°$.

Relative normalization of the spectra was achieved by measuring the beam current in an aligned Faraday cup, with electron suppression, connected to a calibrated current integrator, while continuously monitoring the direction of the beam. Absolute normalization of the cross section was referred to optical-model predictions for the elastic scattering of deuterons on the same target, measured under similar conditions. Figure 2 shows the elastic scattering data in comparison with optical model calculations performed with the parameters of the global prescription of Perey and Perey [13] presented in Table I and also with the prescribed parameters but with the radii r_R and r_I increased by 2% (see further discussion). An error of $\pm 5\%$ is estimated on the absolute cross section determinations.

The experimental angular distribution of the inelastic scattering to the 2_1^+ state is presented in Fig. 3, in comparison with DWBA-DOMP predictions (averaged over spectrograph opening angle). The error bars, where not explicitly shown, are smaller than, or of the order of, the size of the points in the figure and include the combined effect of statistics, plate scanning, and background (and/or contaminant) subtraction, but do not include any error in the absolute cross section scale. Scanning of the emulsion plates under an optical microscope by several calibrated ''readers'' demonstrated a very good reproductibility ($\pm 2\%$) for the number of tracks in each peak. Each spectrum was ''read'' by at least two persons, resulting in low scanning uncertainties.

In perspective, to obtain data with the quality necessary for the proposed CNI studies, for medium mass nuclei, where the interference minimum for deuterons of about 10 MeV appears at relatively forward angles, it is important to apply detection techniques with nuclear emulsions, in association with the excellent beam profile and energy characteristics provided by a Tandem-spectrograph facility.

III. ANALYSIS

The DWBA-DOMP angular distributions shown in Fig. 3 were calculated by means of the code DWUCK4 [14] with the macroscopic collective form factors [4], responsible, respectively, for the Coulomb and nuclear quadrupolar excitation processes:

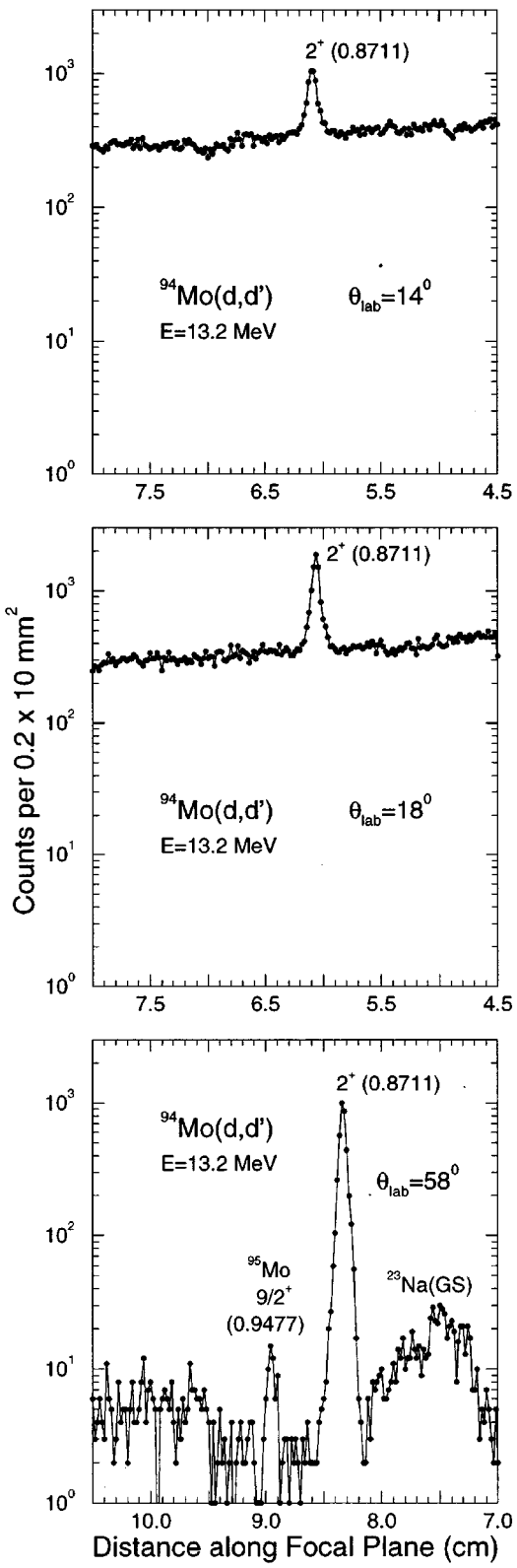

FIG. 1. Portions of the spectra of ^{94}Mo(d,d'), taken at $\theta_{\rm lab}=14°$, 18°, and 58°. Indicated in parenthesis are the energies (in MeV) of the 2_1^+ state in ^{94}Mo [11] and of the contaminant $\frac{9}{2}^+$ state in ^{95}Mo [12]. Observe the very compressed log scale for the y coordinate.

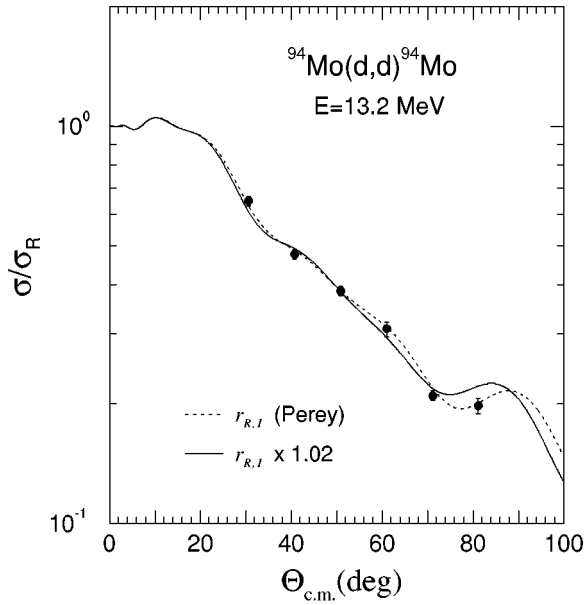

FIG. 2. Elastic angular distribution in comparison with optical model calculations, with parameters of Table I (dashed) and also increasing (see text) both real and imaginary, radii parameters by 2.0% (solid). Experimental uncertainties (error bars) represent the contributions of statistics, plate scanning, and background subtraction.

$$F_2^C(r)=\frac{4\pi e}{5}[B(E2)\uparrow]^{1/2}\frac{1}{r^3} \quad \text{for } r\geqslant R_c=r_cA^{1/3}$$

and

$$F_2^{\rm nuc}(r)=-\delta_R^{\rm pot}(U)\frac{dV(r)}{dr}-i\,\delta_I^{\rm pot}(U)\frac{dW_D(r)}{dr},$$

where V and W_D are the real and surface imaginary depths of the optical potential U, taken with the usual Woods-Saxon and derivative Woods-Saxon forms, with given geometrical parameters (r_R, a_R and r_I, a_I). The parameters δ^C, related to $B(E2)\uparrow$, and $\delta^{IS}=\delta_R^{\rm pot}(U)=\delta_I^{\rm pot}(U)$, related to $B(IS2)$, are, respectively, the charge and isoscalar deformation lengths, to be extracted in the analysis.

Also shown in Fig. 3 are the separated contributions of Coulomb [due to $F_2^C(r)$] and nuclear [due to $F_2^{\rm nuc}(r)$] excitations to the $0_1^+\rightarrow 2_1^+$ transition in ^{94}Mo. Coulomb excitation was treated in the usual way [4] and the spherical Coulomb potential, relative to which the deformation is considered, was taken as that of an uniform charge distribution without diffuseness and radius R_c. The Coulomb form factor was taken as zero inside the sharp cutoff charge radius

TABLE I. Global optical model parameters for elastic deuteron scattering prescribed by Perey and Perey [13]. In the analysis a Coulomb reduced radius of $r_c=1.22$ fm was utilized and r_R and r_I were increased by 2.0%, with respect to the prescription.

V (MeV)	r_R (fm)	a_R (fm)	W_D (MeV)	r_I (fm)	a_I (fm)
96.6	1.15	0.81	17.6	1.34	0.68

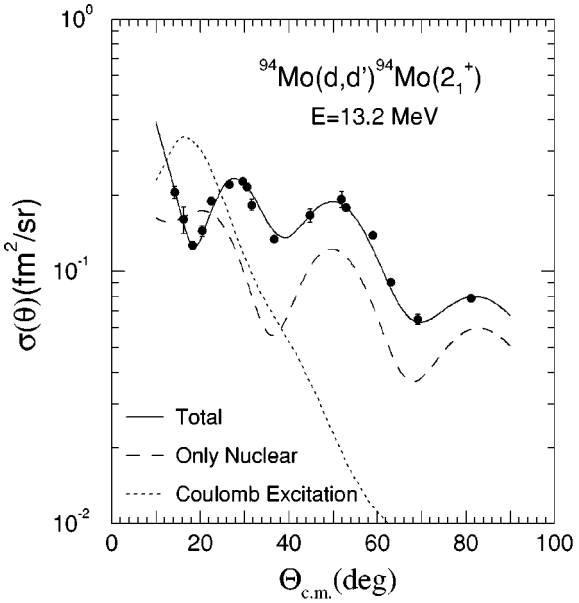

FIG. 3. Experimental inelastic scattering angular distribution used to exemplify the CNI method with deuterons. The solid curve is the best fit of the DWBA-DOMP predictions to the data, while the dotted and dashed ones show the contribution of, respectively, Coulomb and nuclear excitation separately. The parameters of the fit are the potential deformation length δ^{IS}, and the ratio $C = \delta^C/\delta^{IS}$, where δ^C is the charge deformation length. Error bars represent uncertainties due to statistics, plate scanning, and background subtraction and do not include the error in the absolute cross section scale.

and, since this one is well inside the strong absorption radius, the resulting approximation has no appreciable effect on the calculated cross sections. The global parameters which define the optical potential were taken from the well-known systematics of Perey and Perey [13], with a slight modification in the reduced radii to be discussed below.

It is seen that, in particular, the clearly defined interference minimum at $\theta_{\rm lab}\sim 18°$ scales the relative contribution of the two excitation processes and that the absolute cross section values at $\theta_{\rm lab}\geqslant 45°$ are mainly determined by the nuclear excitation. The correlated parameters directly extracted, in a χ^2-minimum fit of the prediction to the data, are δ^{IS} and the ratio $C=\delta^C/\delta^{IS}$, being predominantly influenced, respectively, by the larger angle results and by the pattern of the interference region.

Deuterons are loosely bound projectiles and, as such, subject to absorptive reactions at the very tail of the nuclear potential. This effect is represented in the optical model interpretation through the important role that the imaginary term of the potential plays in determining the pattern of the predicted angular distribution. There are, furthermore, theoretical expectations for possibly different W_D values, even for neighboring nuclei, due to different open reaction channels. The imaginary potential is, therefore, an expected source of uncertainty on the predictions of the model. The reflexes on the extracted deformation lengths of judicious variations of the depth and of the range of the imaginary potential around the globally predicted values [13], besides also of small modifications of the real radius parameter, will be investigated. The main piece of research to be presented in this section is, however, the effect of the known statistical uncertainties of the data on the quantities of physical interest.

A. Reliability of the extracted deformation lengths as a function of some relevant model parameters

In the macroscopic analysis of collective excitations through inelastic scattering, the optical model parameters have a twofold influence on the results: they determine the distorted waves in the entrance and exit channels of the reaction and also the interaction potential in the form factor. To allow for significant comparisons of the spectroscopic information to be extracted through the DWBA-DOMP analysis, in particular if chains of nuclei are to be compared, it seems best to stick, as far as possible, to well-known and approximately constant optical parameter values. This section is devoted to search for the necessity of relaxing this condition, especially for the imaginary term, as dictated by the experimental results. We, therefore, decided to investigate first the reflexes of small modifications of the W_D and r_I, and also of the r_R, parameters (with respect to the global prescription of Perey and Perey [13]) on the theoretical predictions and, in consequence, on the deformation lengths. For now, no other theoretical limitations are considered, so the ensuing discussion is not meant to quantify, in the present stage of the investigation, systematic errors due to a possibly faulty interpretation of the reaction mechanism.

Figure 4 shows, in a comparative way, the effect of modifications in each of the three optical model parameters, which were considered as most relevant, on the quality of the DWBA-DOMP fits to the data of Fig. 3. The vertical axes display $\chi^2_{\rm min}$, the smallest values of χ^2 obtained in adjusting, each time—that is, for each of the several changing values of W_D, r_I, or r_R—the values of δ^{IS} and of the ratio C for best fit. The range of variations of W_D, r_I, and r_R was chosen such as to provide an increase of a factor ~ 4 in $\chi^2_{\rm min}$. The plots in the left column of the figure display $\chi^2_{\rm min}$ as a function of, respectively, the depth of the imaginary surface potential W_D [Fig. 4(a)], the reduced radius r_I of the imaginary potential [Fig. 4(b)], and the reduced radius of the real potential r_R [Fig. 4(c)], maintaining in each case all other optical model parameters fixed at their values of the global Perey and Perey [13] prescription. Arrows indicate the global prescription values of W_D, r_I, and r_R in the figures. The plots in the right column [Fig. 4(d), 4(e), and 4(f)] represent the corresponding results of $\chi^2_{\rm min}$ (attention is called to the expanded vertical scale) for the situation where all parameters, except r_I and r_R, are taken (and fixed if not under study) at their prescribed values, the radii parameters being increased by 2.0%, due to considerations to be presented in what follows. So, Fig. 4(a) displays the values of $\chi^2_{\rm min}$, in a range of up to three times the value of $\chi^2_{\rm min}=117$ obtained at $W_D=17.2$ MeV. It is seen that $W_D=17.6$ MeV (see arrow) of the Perey and Perey prescription [13] is included in the ''bottom'' of the curve. Figures 4(b) and 4(c) indicate, on the other hand, that the respective minima of $\chi^2_{\rm min}$ occur, for both radii, at values which are about 2% higher than the prescription [13]. Figure 4(c) furthermore tells us that an important reduction is achieved in $\chi^2_{\rm min}$, especially through the modification of the real reduced radius r_R. It may, thus, be noted that, contrary to expectations, the imaginary term

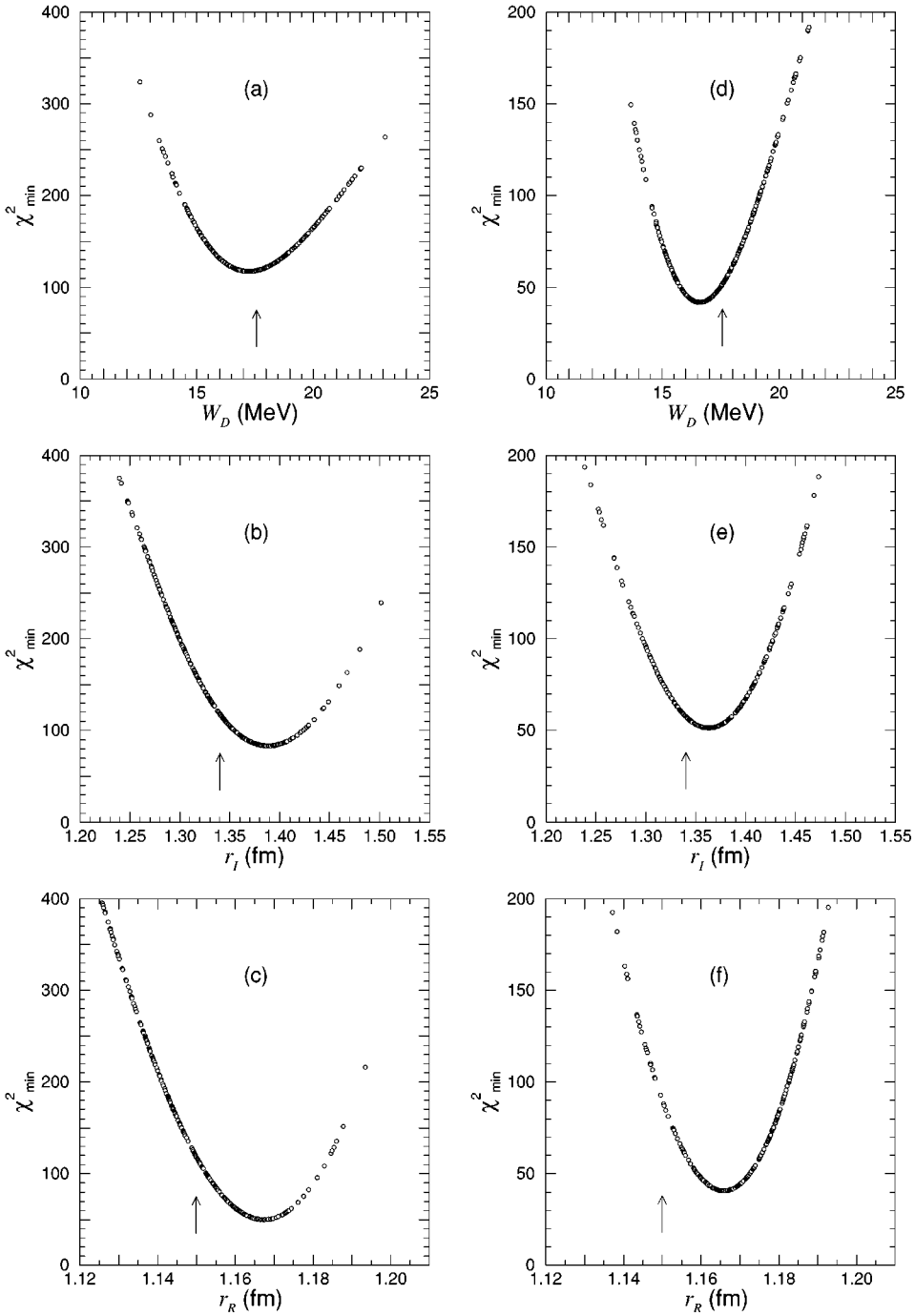

FIG. 4. Variation of the quality of the fit to the data of Fig. 3, as three optical parameters (W_D, r_I, and r_R), each at a time, are removed from their globally prescribed [13] values, indicated by arrows (see text). In (a) to (c), the parameters which were not under study were maintained fixed at their globally [13] prescribed values; in (d) to (f), the same procedure was adopted, but the r_R and r_I parameters, when fixed, were increased by 2.0% with respect to the prescription.

W_D of the global parameters of Perey and Perey [13] reproduces the data rather well. On the contrary, the 2% increase in r_R is essential to adjust the relative phase of the prediction to the data, since the real radius has, as is well known, a predominant influence on the width of the diffractive oscillations of the angular distribution. This effect is responsible for the reduction of a factor ~ 2 in $\chi^2_{\min}$ shown in Fig. 4(c). In fact, direct inspection of the experimental results under consideration and also of those for the same reaction at 16.0 MeV deuteron energy and for the other isotope ^{98}Mo (at both energies) [15] had already shown the inelastic diffractive oscillations to correspond to an apparently larger object than appropriate for the representation of the elastic results. This may denote some particularity of the reaction mechanism for the weakly bound deuteron (since it was not observed with α's) which is beyond the DWBA-DOMP representation, but is stable with respect to deuteron energy and nuclear mass in the investigated region. Therefore, in the analysis of these CNI studies with deuterons on Mo, an option was made to modify both, the real and imaginary radii, by an increase of 2.0% with respect to the global prescription [13], in view also of maintaining their relative value. All other optical parameters, also W_D, were kept as globally prescribed, in accordance with the philosophy of aiming at an as uniform description of the intervening reaction mechanism for the whole mass region, as the data will allow for.

Figure 5 resumes, on one plot, the physical information associated to the right column of Figs. 4(d)–4(f). The three trajectories there displayed correspond, each, to the sequence of pairs (δ^{IS},C), determined by the best-fitting procedure

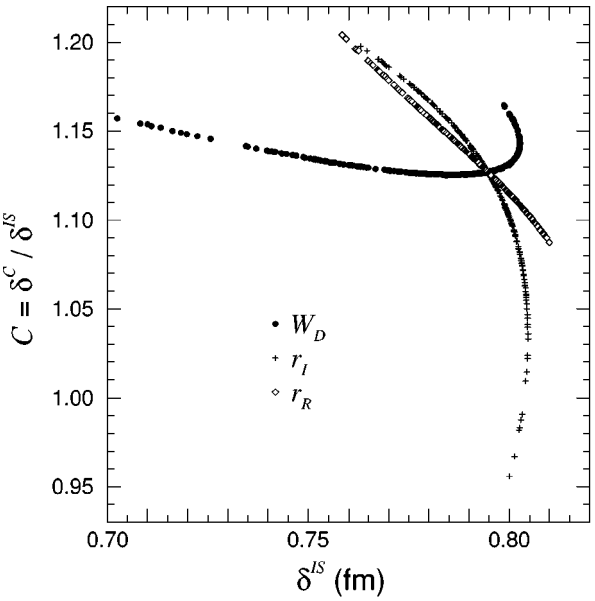

FIG. 5. Sequences of (δ^{IS},C) pairs obtained in the minimizing procedures represented in Figs. 4(d), (e), and (f), for each of the three selected optical model parameters (W_D, r_I, and r_R). The point of intercept correspond to the values of δ^{IS} and C taken to be the results of the present analysis (see text).

already described, with the several values of, respectively, W_D, r_I, and r_R. The particular points plotted in this figure are the result, as they are in Fig. 4, of Monte Carlo chosen values of the optical parameters around their globally prescribed [13] values. An inspection of Fig. 5 tells immediately the regions of variability of δ^{IS} and $C=\delta^C/\delta^{IS}$ associated with indeterminations in the here highlighted optical model parameters. It is seen that the radii and W_D have orthogonal effects on the physical results: the last one corresponds to a rather sharp value of C and a relatively large interval for δ^{IS}, while the contrary is verified for variation in the radii. The point of intercept in the figure is the value obtained for δ^{IS} and C with all the optical parameters of the DWBA analyses taken at their globally prescribed [13] values, except for the mentioned 2.0% increase in r_I and r_R. A similar figure constructed for the results displayed in the left part of Figs. 4(a)–4(c) contains no additional information of physical interest, except that the trajectory in the (δ^{IS},C) plane for varying W_D has a still smaller slope, the point of intercept corresponding to $\delta^{IS}=0.78$ fm and $C=1.15$.

The behavior of the trajectories in the (δ^{IS},C) plane is in accordance with the *a priori* known effects of the optical parameters on DWBA-DOMP predictions. In fact, W_D is known to affect the ''peak'' to ''valley'' ratio of the diffractive oscillations, higher values of W_D filling in the valleys progressively and washing the peaks out, resulting in higher δ^{IS} values, while the interference minimum remains about the same for constant C. On the other hand, the radii, particularly the real one, modify the proper diffraction pattern with respect to the angular scale, affecting especially the value of C. It is seen, through Figs. 4 and 5, that the enormous increase of a factor of 4 in the $\chi^2_{\min}$ values corresponds, in total, to a variability interval of no more than $\pm 10\%$ in the relevant physical quantities δ^{IS} and C. It seems, thus, qualitatively justified that significant physical information can be extracted, even if the optical model parameters are put under restricted doubt.

The Monte Carlo choosing applied here to three of the optical parameters is part of a study, which is still under way, to associate a total model uncertainty to the deformation lengths, and will be the subject of a forthcoming publication [16]. In fact, it is our intention, in the long run, to be able to extract a kind of error belt around the theoretical predictions, reflecting the analysis of the several theoretical shortcomings, with a hopefully increasing degree of completeness.

B. Uncertainties of the deformation lengths due to experimental errors

This section is devoted to discussing the influence of the experimental errors on the derived quantities of physical interest and their uncertainties. A systematic error on the absolute cross section scale, estimated to be less than 5%, affects exclusively δ^{IS} and not the ratio C and will not be considered in this section. The statistical errors, on the other hand, affect both parameters of interest. The error bars shown in Fig. 3 are representative of standard deviations on the data points. In the extraction of confidence intervals for the fitted parameters, the nuclear physics literature frequently registers the application of two misused recipes: the simple addition of 1 to the value $\chi^2_{\min}$, with all, but the one parameter under consideration, fixed at the values of the best fit or, worse, the increase of 10% to $\chi^2_{\min}$, both thought as defining the confidence interval of each parameter, for 68.3% of expectation. The first recipe is adequate only if a single free parameter is considered [9], while the second one is at best an approximation to the first, when about ten data points are available and agreement with the theoretical prediction is statistically perfect.

The statistically recommended procedure depends on the number of free parameters. Furthermore, if the parameters are correlated and/or if the model predictions are not linear in the parameters, as is the case for δ^{IS} and C, special care must be taken if any numerical manipulation involving both is to be done and the stability of the results is to be investigated. In particular, if δ^C is to be determined, the correlation has to be explicitly taken into account. For this purpose, general techniques have been brought forward by Cline and co-workers [17], in the extraction of electromagnetic matrix elements in multiple Coulomb excitation of nuclei, and by Lampton, Margon, and Bowyer [18], in a more detailed form, within their astrophysical research projects, the last being systematized only recently, among other issues, by Press *et al.* [9], in a successful book. The recommended procedure is to define the hypervolumes in the space of the interesting parameters which contain the expected amounts of events. The contours of these volumes are obtained by specifying predetermined values for $\Delta\chi^2$ to be added to $\chi^2_{\min}$, all the parameters being allowed to vary freely. The values of $\Delta\chi^2$ depend on the statistical confidence level (for instance 68.3%, 99.7%, etc.) and on the number of parameters. For two parameters, which is the case of the present example, the contour lines are not exactly elliptical curves in the plane (δ^{IS},C), since the model is not linear in both parameters. Another critical point is that $\chi^2_{\min}=51.5$, for the 17 experimental points of the example, leads to $\chi^2_{\text{red}}=3.43$,

clearly indicating differences between data and model prediction in excess of the statistical expectation for normally distributed data, although these values of $\chi^2_{\rm red}$ may be considered typical for DWBA-DOMP fits with global parameters. These facts point to the convenience of a thorougher investigation of the statistical procedures.

Entering in detail, when two parameters are considered, the Lampton, Margon, and Bowyer recipe, as cited by Press *et al.* [9], specifies that the regions which should contain 68.3 and 99.7% of the statistically expected events for normal data and perfect fit are bounded by the approximately elliptical contour lines obtained considering $\Delta\chi^2$ of 2.3 and 11.8, respectively. In Fig. 6(a) these contour lines, obtained for the example under discussion, are represented by the two outermost solid curves. Focusing on the 68.3% region, it follows that the projections of this contour on each axis corresponds to approximately two times 1.5σ [18] of the respective parameter. That is, if both parameters are looked upon jointly, the projection of the 68.3% region exceeds necessarily the value of 2σ. If, on the other hand, the information needed refers to the uncertainty in one parameter of the fit, whatsoever the value of the other (which is thereby relaxed), slices of widths $\sim 2\sigma$ are defined in the plane (δ^{IS}, C) corresponding to the projection of the contour line of $\chi^2_{\rm min}+1$ (represented in the figure by the inner solid almost elliptical curve). The referred slices are limited in Fig. 6(a) through small-dotted vertical and horizontal lines.

A frequently employed χ^2 minimizing procedure is the Gauss-Marquardt method, due to its rapid convergence properties. This method was, in fact, applied to obtain $\chi^2_{\rm min}$ and the uncertainties of the parameters in the form of a covariance matrix, which contains all the relevant information, as long as the linear approximation is adequate. In this case, exact ellipses of constant χ^2 are defined around $\chi^2_{\rm min}$, which are function solely of the values of the standard deviations of the parameters and their correlation. These are shown as dotted curves in Fig. 6(a) and, for the relatively well-behaved case taken as example, they are seen to be very similar to the contour lines with the same $\Delta\chi^2$ values. Within the linear approximation, it may be shown [18] that the projections of the two inner ellipses on each parameter axis correspond exactly to twice 1.515σ and 1.000σ, respectively.

Now, as already stated, perfect fit of the CNI data is not expected nor obtained with DWBA-DOMP and global optical parameters. However, if the aim is on comparative studies of collective properties of nuclei, as will be further justified in the discussion, it is this kind of global analysis which is deemed as the most appropriate fit to CNI data. Furthermore, the most interesting parameter for these studies, C, is derived almost exclusively from the forward angle data points and may, in other situations, have an expressive nonlinear effect on the fit. It is, therefore, important to bear in mind that the linearization procedure employed in the Gauss-Marquardt approach may under circumstances not be the best method to trust. The Lampton, Margon, and Bowyer procedure [18], which is not restricted to linear dependence on the parameters, is clearly to be preferred. The general techniques discussed so far do, however, not address the issue for model and data in poor statistical accord. In order to verify the validity, of these techniques [9,17,18] for the CNI data under study, a direct statistical test was decided upon,

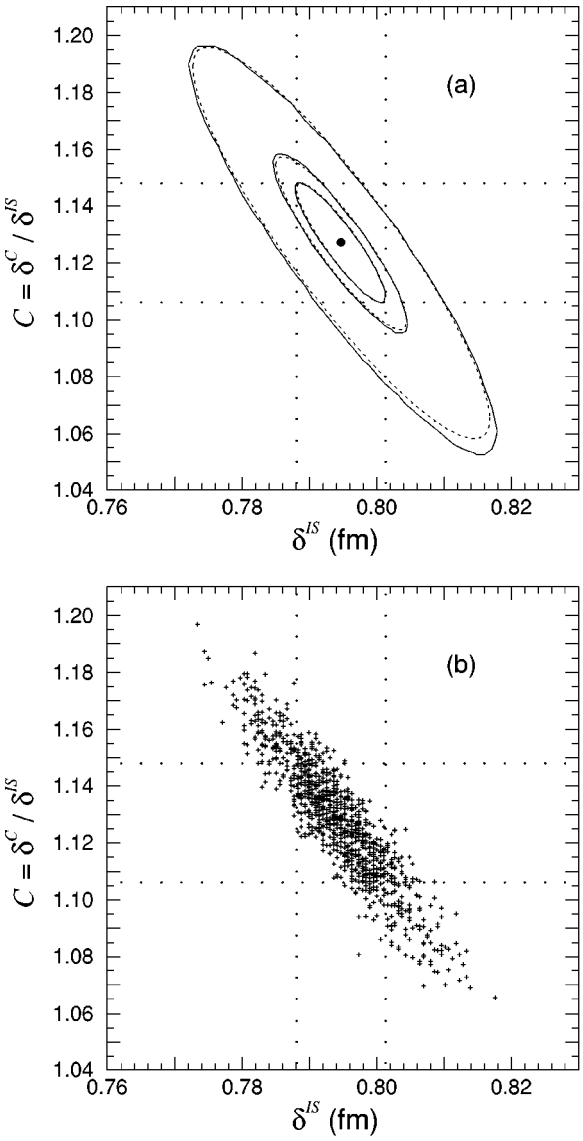

FIG. 6. (a) Best fit values of δ^{IS} and C for the experimental results presented in Fig. 3, with confidence region contours and ellipses: the solid curves are the constant χ^2 contour lines [9], while the dotted ones correspond to equivalent ellipses calculated from the Gauss-Marquardt parameters, both corresponding to statistical expectations of, respectively, 39.3% ($\chi^2_{\rm min}+1$), 68.3% ($\chi^2_{\rm min}+2.3$), and 99.7% ($\chi^2_{\rm min}+11.8$) of the events. (b) Monte Carlo simulated results with 1002 trials on 17 fictitious ''data'' points, produced starting from the 17 actual experimental points. For each simulated ''angular distribution'' the minimum χ^2 was found and the corresponding values of δ^{IS} and C are represented as crosses in the (δ^{IS}, C) plane. Small-dotted vertical and horizontal lines in both (a) and (b) limit the slices which correspond, respectively, to 2σ of δ^{IS} and C.

through Monte Carlo simulations of ''new'' data. This statistical procedure is mathematically known to provide equivalent results, for Gaussian data distributions and perfect model fit. It is not *a priori* evident, on the other hand, if this property is maintained for the case under study, in particular, if any idiosyncrasy should be present in the experimental points. Figure 6(b) is the representation of the 1002 results obtained by Monte Carlo simulations of, each time, a ''new angular distribution'' containing 17 fictitious ''data'' points,

TABLE II. Results of the statistical analysis of DWBA-DOMP fits to the angular distribution of ^{94}Mo(d,d') presented in Fig. 3. The second and third columns contain numerical information associated with Fig. 6(a) and the last two columns with Fig. 6(b).

Parameters of physical interest	Experimental best fit		Monte Carlo simulation[a]	
	Gauss-Marquardt method	Contour line method	m	s
δ^{IS} (fm)	0.7947(64)	0.7947(66)	0.7942	0.0069
C	1.127 (20)	1.127 (21)	1.129	0.022
δ^{C} (fm)	0.896 (10)	0.896 (11)	0.896	0.011
r	−0.899	−0.904	−0.910	
$P(A_1)$	64.9%	66.7%	68.7%	
$P(A_2)$	93.1%	95.1%	95.5%	
$P(A_3)$	99.6%	99.7%	99.9%	

[a]m: mean value; s: standard deviation.

produced starting from the actual 17 experimental points, and choosing in accordance with Gaussian distributions defined by the experimental standard deviation of each point. For each simulated ''angular distribution'' the $\chi^2_{\min}$ was found and the corresponding values of δ^{IS} and C are represented as crosses in Fig. 6(b). It may be qualitatively appreciated that the crosses are distributed in the manner expected in behalf of the ellipses of Fig. 6(a), that is, almost all are contained within the outer ellipse, while about 2/3 are inside the middle one. Figure 6(b) also helps in making the meaning of the 2σ slices clear. Take, for instance, the horizontal slice which defines the 2σ interval for the C parameter. Comparing Fig. 6(a) with 6(b), it is seen that, since no restriction is made to δ^{IS}, crosses outside the 68.3% ellipse, but within this slice, are counted to complete the 68.3% expectation for C.

Table II presents in the first three lines the parameters of physical interest, as determined from the Gauss-Marquardt and contour line methods, also in comparison with the mean values (m) of the 1002 Monte Carlo results. The standard deviations, $\sigma_{\delta^{IS}}$ and σ_C, associated to the best fit values are given in parentheses, while the corresponding values (s) obtained from the Monte Carlo distribution are shown in the last column of Table II. In the present well-behaved example, where the data are good enough to restrict the parameters of the fit to only small variations around the ''best values,'' the dependence may be considered as almost linear and the values came out very similar.

With the intention of better appreciating the quantitative statistical content of Fig. 6, a counting procedure of the crosses was executed, as a first step considering ellipses constructed with the proper mean values, standard deviations and correlation coefficient from the Monte Carlo simulations. A convenient way to represent the ellipses of constant probability density, for two correlated parameters obeying a Gaussian distribution, is through the constant A, given by

$$A^2=\left[\frac{\delta^{IS}-\langle\delta^{IS}\rangle}{\sigma_{\delta^{IS}}}\right]^2-2r\left[\frac{\delta^{IS}-\langle\delta^{IS}\rangle}{\sigma_{\delta^{IS}}}\right]\times\left[\frac{C-\langle C\rangle}{\sigma_C}\right]+\left[\frac{C-\langle C\rangle}{\sigma_C}\right]^2,$$

where $\langle\delta^{IS}\rangle$ and $\langle C\rangle$ are the mean (m) or the best fit values, $\sigma_{\delta^{IS}}$ and σ_C (standing also for s) are the standard deviations and r is the Pearson correlation coefficient between δ^{IS} and C. Figure 7 represents, as a function of A (calculated with the values of the two last columns of Table II), through a histogram, the relative frequency of crosses, per unit area (in each of the successive elliptical crowns), which is the physical approximation to the probability density dP/dS. Also shown in the figure is the expected probability density distribution. The good accordance lends support to the statistical assumptions made and demonstrates the internal consistency of the Monte Carlo procedure. The three last lines in the fourth column of Table II show the summed relative

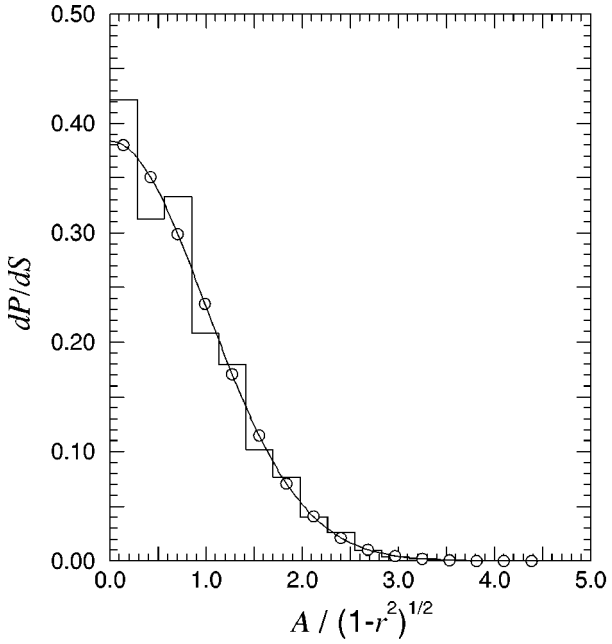

FIG. 7. Histogram of the probability density distribution as a function of the parameter A defined in the text, extracted for the Monte Carlo simulations presented in Fig. 6(b). The relative frequency was obtained counting the number of crosses contained in each of the successive elliptical crowns and normalizing per unit area and total number of events. In comparison, a Gaussian with $\sigma_0=1$ in the units of the horizontal axis, corresponding to the statistical expectation for a correlation coefficient of $r=-0.910$, is also shown as solid curve.

frequencies, $P(A)$, for the Monte Carlo results, up to values A_1, A_2, and A_3, which should theoretically correspond to probability contents of respectively 68.3, 95.4, and 99.7%, and are seen to be in extremely good agreement with these expectations. To complete the quantitative analysis, the counting procedure of the Monte Carlo results was also undertaken considering the Gauss-Marquardt ellipses and contour lines of interest, registering the crosses inside the respective curves characterized by the A_1, A_2, and A_3 values. It is to be remembered that two of these ellipses and contour lines, corresponding to A_1 and A_3, are shown as, respectively, dotted and solid lines in Fig. 6(a). The last three lines, in the second and third columns in Table II, present the statistical content $P(A)$ for the three ellipses and contour lines and it may be appreciated that the simulation came, within the statistical uncertainty inherent to determinations which start from only 17 experimental points, very close to the expected values [19]. It may, however, also be appreciated that the Gauss-Marquardt results are, in particular for the 68.7% ellipse, some 6% lower than the expectation. This situation will be intensified when data with larger error bars, or with insufficient definition of the crucial minimum, allow for farther excursions with respect to the ''best'' fit values, evidencing, thus, the known nonlinearities of the fitting function. In all, the comparative analysis of the physical information contained in Table II definitely shows, for the present example, the very good quantitative agreement of the three statistical procedures here adopted, demonstrating the basic equivalence of them. The adequacy of the Press *et al.* [9] recipe seems thus established also for the here considered CNI measurements with DWBA-DOMP fits. Whenever the constant χ^2 contour lines prove adequate resemblance with the corresponding ellipses characterized by A_1, A_2, and A_3 of the Gauss-Marquardt result, the uncertainties may be extracted directly from the covariance matrix. If, in other experimental situations, important differences between the two representations should show up, indicating perceptible influences of the nonlinearity, the contour line method [9] is recommended and comparison between experimental results can, in principle, only be made through direct inspection of the confidence regions in parameter space. In very suspect cases, other Monte Carlo simulations may be in order. Any important differences of these with respect to the contours may be indicative of trouble with the best fit.

Two more Monte Carlo simulations performed (with $N=999$ and 1000) confirm, in the present test case, besides the expected stability of the results, that the fluctuations, measured through the standard deviations s, are systematically about 10% larger for the simulations in comparison with the Gauss-Marquardt values.

The statistical analysis instills confidence on the experimentally attributed uncertainties up to two significant figures. Therefore, from this point of view, the ratio C, in an experimental situation like that of Fig. 3, can be determined on a 2% precision level (see Table II). The nuclear deformation length, on the other hand, can through inelastic deuteron scattering be obtained with an about 1% statistical uncertainty, as can be also appreciated in Table II. The value of $\delta^C = C\,\delta^{IS}$ is accompanied by an statistical uncertainty smaller than that of the C value, since the negative covariance was taken into due account in the error propagation. The quadratic relationship reflects the quoted experimental (only statistical) uncertainties as $\pm 1.6\%$ in $B(IS2)$ and $\pm 2.2\%$ in $B(E2)$.

IV. DISCUSSION AND CONCLUSIONS

The statistical analysis applied in Sec. III has demonstrated that inelastic scattering studies with deuterons of ~ 13 MeV, on intermediate mass nuclei, may result, for the 2_1^+ excitations, in $B(IS2)$ and $B(E2)$ values on the few percent precision level. The accuracy, on the other hand, should be examined from a complementary perspective. The quantity of primary interest for several nuclear structure interpretations is the ratio of the reduced transition probabilities $B(E2)$ and $B(IS2)$, which, for CNI data, is more accurate than either quantity separately, since obtained from the same measurement. In fact, in this experimental situation, the cross section scale errors are canceled and some of the model errors in the analysis are diluted, in particular, those associated with known limitations of the distorted waves in the DWBA analysis.

In the ratio

$$\frac{B(E2)}{B(IS2)} = e^2\left(\frac{\delta^C}{\delta^{IS}}\right)^2\left[\frac{R_c}{R_m}\right]^2 = e^2\left(C\,\frac{r_c}{r_m}\right)^2,$$

besides the uncertainty in C, only the uncertainties in the reduced charge r_c and mass r_m radii have to be considered, if absolute values of the ratio are needed. In the present method of analysis, a reduced charge radius of $r_c = 1.22$ fm was used for the sharp cutoff spherical charge distribution, in accord with electron inelastic scattering and muonic atom data, as catalogued by Elton [20], Barret and Jackson [21], and de Vries *et al.* [22], when reduced to sharp-edge distributions. The reduced radius of the mass distribution is suggested to be taken as $r_m = 1.16$ fm, which is obtained from the value of Chung and Myers [23], also transformed to a sharp edge interpretation. Should the reduced radii be uncertain by as much as 5% each, a less than 15% systematic uncertainty would result on the ratio of the two reduced transition probabilities of interest. Otherwise, if chains of nuclei are studied in a comparative way, only the relative values of $B(E2)$ and $B(IS2)$ may be of importance and thus systematic errors such as those on the radii are irrelevant. It suffices, then, to be sure that the quantities C, for the several nuclei to be compared, were extracted in a consistent way. As formerly stated, optical parameters influence DWBA-DOMP results in a twofold manner, being responsible for the distorted waves and for the nuclear form factor of the transition. Whenever the experimental findings are not frontally misrepresented by the parameters of a global prescription, these are felt to provide the best choice for systematic spectroscopic analyses, since in this case the chain of nuclei is represented on the same footing. Comparison can thus be made, as is necessary, on the few percent level, due only to the statistical uncertainty in C, which was shown, in Sec. III B, to be determinable within 2%, under the present experimental conditions. It is to be remembered that C gives direct information on the ratio of proton to neutron quadrupolar moments of the 2_1^+ excitation, $C = 1.00$ being the limiting value between proton/neutron contributions exceeding ($C > 1.00$) or lacking (C

TABLE III. Results of the experimental best fit and the fit obtained with δ^C fixed at the Raman *et al.* [5] value.

Fit[a]	δ^{IS} (fm)	C	δ^C (fm)	$\chi^2_{\min}$	χ^2_{red}
Experimental best fit	0.7947(66)	1.127(21)	0.896(11)	51.51	3.43[c]
Fixed δ^C	0.8345(57)	0.971(14)	0.810(8)[b]	102.20	6.39[d]

[a] $r_R = 1.173$ fm and $r_I = 1.367$ fm; all other optical parameters at their prescribed [13] values.
[b] Deduced from the value adopted for $B(E2)$ by Raman *et al.* [5].
[c] Degrees of freedom $= 17 - 2 = 15$.
[d] Degrees of freedom $= 17 - 1 = 16$.

<1.00) with respect to the homogeneous Z/N value, expected for purely collective states [4].

Finally, what further concerns the accuracy of the absolute values of $B(E2)$ and $B(IS2)$ separately, from an experimental point of view not more that about 5% of absolute error is estimated on the cross sections and, if we stick to the chosen theoretical description and globally prescribed parameters, the preliminary analysis of the influence of some model parameters, presented in Sec. III A, is also not indicative of great variability. Of course, nothing can, for now, be said about systematic errors due to any fault in the representation of the reaction mechanism through the chosen DWBA-DOMP approach. Data taken at other incident deuteron energies and also with other projectiles may, in the future, offer clues on that.

Table III summarizes the results derived from the contour line recipe, taken as the final values of the analysis effectuated on the ^{94}Mo$(d,d')^{94}$Mo(2_1^+) reaction at 13.2 MeV. Also shown in Table III, for the sake of completeness, are the results of calculations (see Fig. 8), which tried to force, within the adopted methodology, a fit on the data taking the prefixed value of $\delta^C = 0.810$ fm, in correspondence to the adopted $B(E2)$ for ^{94}Mo of the Raman *et al.* [5] compilation. As may be seen in Fig. 8 and through the $\chi^2_{\min}$ values of Table III, a considerably worse description of the experimental data is thereby obtained, in particular, in the interference region. This is not to be taken as implying that our value for δ^C is to be preferred to the one adopted [5], since, as stated, systematic errors may intervene, but in our view confirms the

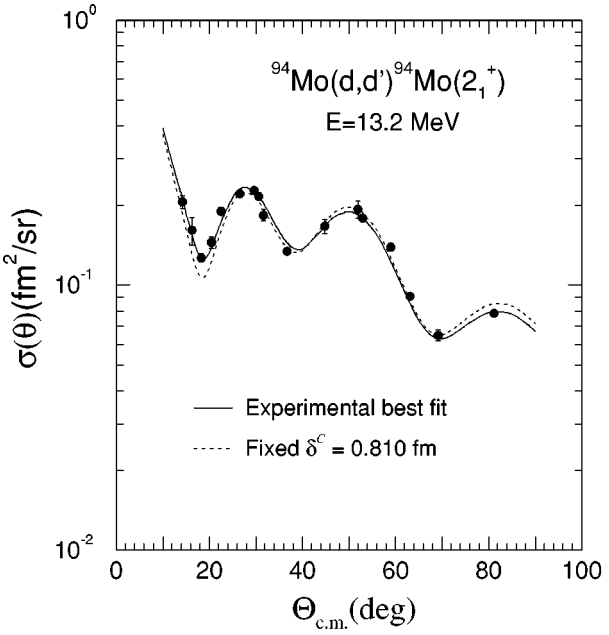

FIG. 8. Comparison between experimental best fit and a fit obtained with δ^C fixed at the Raman *et al.* [5] value.

value of $C \sim 1.1$. The analysis of data obtained for the same scattering at 16.0 MeV incident energy gives results which are basically consistent with the information here presented for 13.2 MeV. It is, therefore, argued that the CNI measurements, through the value of C, disclose the proton contribution to 2_1^+ excitation to be slightly more important than the neutron one in the case of the first quadrupolar excitation of ^{94}Mo, in the very contrast to what was observed [7] for its isotone, ^{92}Zr, where $Z = 40$ acts as if closed, resulting in a clear predominance of the neutrons in the 2_1^+ excitation.

ACKNOWLEDGMENTS

The authors are indebted to M. D. L. Barbosa for his contributions during several phases of the present work. Financial support by CNPq (Conselho Nacional de Desenvolvimento Científico e Tecnológico), FINEP (Financiadora de Estudos e Projetos), and FAPESP (Fundação de Amparo à Pesquisa do Estado de S. Paulo) is gratefully acknowledged.

[1] A. Bohr and B. R. Mottelson, *Nuclear Structure* (Benjamin, New York, 1975).
[2] M. M. Gazzaly, N. M. Hintz, G. S. Kyle, R. K. Owen, G. W. Hoffmann, M. Barlett, and G. Blanpied, Phys. Rev. C **25**, 408 (1982).
[3] A. M. Bernstein, V. R. Brown, and V. A. Madsen, Phys. Lett. **71B**, 48 (1977); **103B**, 255 (1981).
[4] G. R. Satchler, *Direct Nuclear Reactions* (Claredon, Oxford, 1983).
[5] S. Raman, C. H. Malarkey, W. T. Milner, C. W. Nestor, and P. H. Stelson, At. Data Nucl. Data Tables **36**, 1 (1987).
[6] L. C. Gomes, L. B. Horodynski-Matsushigue, G. M. Ukita, J. L. M. Duarte, and T. Borello-Lewin, XV Reunião de Trabalho em Física Nuclear no Brasil, Caxambu, 1992 (unpublished), p. 69; L. C. Gomes, L. B. Horodynski-Matsushigue, T. Borello-Lewin, J. L. M. Duarte, and G. M. Ukita (unpublished).
[7] L. B. Horodynski-Matsushigue, T. Borello-Lewin, and J. L. M. Duarte, XVI Reunião de Trabalho em Física Nuclear no Brasil, Serra Negra, 1993 (unpublished), p. 61; Proceedings of the International Nuclear Physics Conference, São Paulo, Brazil, 1989 (unpublished), Vol. I, p. 309.
[8] G. M. Ukita, L. C. Gomes, J. L. M. Duarte, L. B. Horodynski-Matsushigue, M. D. L. Barbosa, and T. Borello-Lewin, XVII Reunião de Trabalho em Física Nuclear no Brasil, Angra dos Reis, 1994 (unpublished), p. 48; T. Borello-Lewin, G. M. Ukita, J. L. M. Duarte, L. B. Horodynski-Matsushigue, L. C.

Gomes, and M. D. L. Barbosa, International Conference on Nuclear Dynamics at Long and Short Distances, Angra dos Reis, Brasil, 1996 (unpublished), p. 19.
[9] W. H. Press, B. P. Flannery, S. A. Teukolsky, and W. T. Vetterling, *Numerical Recipes* (Cambridge, New York, 1990).
[10] D. Pulino, G. M. Sipahi, G. M. Ukita, T. Borello-Lewin, L. B. Horodynski-Matsushigue, J. L. M. Duarte, W. G. P. Engel, and J. C. de Abreu, Rev. Bras. Aplicações Vácuo **10**, 87 (1991).
[11] J. K. Tuli, Nucl. Data Sheets **66**, 1 (1992).
[12] T. W. Burrows, Nucl. Data Sheets **68**, 635 (1993).
[13] C. M. Perey and F. G. Perey, At. Data Nucl. Data Tables **17**, 1 (1976).
[14] P. D. Kunz, computer code DWUCK4 version, Colorado University, 1974 (private communication).
[15] G. M. Ukita *et al.* (unpublished).
[16] J. L. M. Duarte *et al.* (unpublished).
[17] D. Cline, Annu. Rev. Nucl. Part. Sci. **36**, 683 (1986); D. Cline and P. M. S. Lesser, Nucl. Instrum. Methods **82**, 291 (1970); T. Czosnyka, D. Cline, L. Hasselgren, C. Y. Wu, R. M. Diamond, H. Kluge, C. Roulet, E. K. Hulet, R. W. Lougheed, and C. Baktash, Nucl. Phys. **A458**, 123 (1986).
[18] M. Lampton, B. Margon, and S. Bowyer, Astrophys. J. **208**, 177 (1976).
[19] A. Stuart, J. K. Ord, and M. Kendall, *Advanced Theory of Statistics* (Griffin, London, 1987).
[20] L. R. B. Elton, *Nuclear Sizes* (Oxford University Press, New York, 1961).
[21] R. Barret and D. F. Jackson, *Nuclear Sizes and Structure* (Claredon, Oxford, 1979).
[22] H. de Vries, C. W. de Jager, and C. de Vries, At. Data Nucl. Data Tables **36**, 495 (1987).
[23] H. S. Chung and W. D. Myers, Nucl. Phys. **A451**, 283 (1990).